Dissipation by transfer and its influence on barrier distributions

G. Colucci,[1,*] E. Piasecki,[1] A. Trzcińska,[1] P. W. Wen,[2] V. Palmin,[3] and T. Abramova[3]
[1]*Heavy Ion Laboratory, University of Warsaw, 02-093 Warsaw, Poland*
[2]*China Institute of Atomic Energy, Xinzhen, Fangshan, Beijing 102413, China*
[3]*Moscow Institute of Physics and Technology, Moscow 117303, Russia*

(Received 21 February 2024; accepted 3 June 2024; published 27 June 2024)

The quasielastic barrier distribution (D_{qe}) of the $^{20}Ne + ^{208}Pb$ system exhibits a single broad structureless peak, unlike the results of coupled-channels calculations, including the strongest collective states of both projectile and target, which show a pronounced double-peaked structure. Separate measurements of the transfer strength, combined with the relatively small number of weak noncollective states in ^{208}Pb, suggested that the observed barrier smoothing in this system could be due to the influence of couplings to transfer reactions. The coupled reaction channels (CRC) calculations performed by explicitly coupling to the two strongest transfer partitions, one-neutron pickup and one-proton stripping, suggest that the cumulative effect of coupling to many relatively weak transfer channels is responsible for the barrier smoothing rather than a few strong transfer reactions. In this perspective, the four main transfer channels (one- and two-neutron pickup and one-proton and one-alpha stripping) of the $^{20}Ne + ^{208}Pb$ system were coupled to the collective excitations by employing an upgraded CCQEL code, where we introduced the dependence of the transfer coupling strength on the transferred particle and experimental Q-value distributions. Because of the availability of Q distributions measured at the two beam energies of 96 and 103 MeV, two sets of transfer coupling strength were determined for each transfer channel. The study with the upgraded code indicates transfers with negative ground-to-ground states Q value as the leading cause of the smearing of the barrier distribution. At the beam energy of 103 MeV, the smoothing of D_{qe} is influenced mainly by the one-neutron pickup. On the other hand, the one-neutron pickup and one-proton stripping transfers are dominant for the beam energy of 96 MeV. These results highlight the importance of the transfer coupling dependence on the experimental Q-value distribution and, consequently, on the dissipation of the projectile kinetic energy.

DOI: 10.1103/PhysRevC.109.064625

I. INTRODUCTION

Determination of the barrier distributions is an excellent tool for revealing details in the energy dependence of the measured fusion cross sections at energies close to the Coulomb barrier. During fusion reactions, the excited states of the projectile and target nuclei get populated complexly, and their relative motion couples with them. The study of the influence of a small number of projectile and target collective excitations on near- and sub-barrier fusion was successfully addressed by the coupled channels (CC) method [1,2]. As a result, the barrier distribution structures are interpreted as a fingerprint of the structure of the interacting nuclei.

Although the CC method successfully explained the substantial enhancement of sub-barrier fusion cross sections as well as the observed structures in the barrier distributions [1], several experiments revealed that the barrier distributions of some systems get distorted, or the structure gets completely blurred in comparison with theoretical predictions [3,4]. This behavior seems to result from dissipation: the partial conversion of the projectile-target kinetic energy into their heating. This phenomenon is a topic much less understood. There are two main mechanisms of dissipation: excitation of noncollective levels by nuclear and electromagnetic interactions [3–6] and mutual projectile-target transfer of light particles. The first one has been treated by combining the CC method with the random matrix theory (CCRMT model), with promising results [4,7,8]. The influence of transfer was both experimentally and theoretically investigated, but the conclusions are still contradictory [9–26]. Because of the complicated nature of this many-body time-dependent phenomenon, the theoretical interpretation is arduous, requiring both unknown information and enormous computer calculation power. These difficulties force the introduction of approximations into the models, which might considerably influence the results. Generally, two approaches address the problem: microscopic and macroscopic (phenomenological). The first is used, e.g., in the program FRESCO [27]. In principle, the code can describe the transfers and their influence on fusion and quasielastic scattering of ions; however, it requires precise information on nuclear structure and complicated couplings of transfer channels, particularly when multistep transfers are possible.

*Contact author: colucci@slcj.edu.pl

Because of this, there have been few attempts to employ this approach to calculate barrier distributions, particularly for medium and heavy systems. We are aware of only a few successful applications of FRESCO for barrier distribution estimations for not-very-light systems, mainly performed by the Brazilian group [28]. However, they focused on systems for which the barrier distributions are of the Gaussian-like shape, therefore without the possibility of observing changes in their structure.

The measurement of the quasielastic barrier distribution $D_{\rm qe}$ for the ^{20}Ne + ^{208}Pb system [29] found a single broad structureless peak, in marked contrast to the results of coupled-channels calculations, including couplings to the strongest collective states in both projectile and target, which showed a pronounced double-peaked structure. A similar situation concerns the ^{20}Ne + ^{92}Zr system, which also shows a broad structureless peak in the experimental $D_{\rm qe}$ [3], unlike the results of coupled channels calculations.

In Ref. [3], we conjectured that because the ^{92}Zr nucleus has many weakly coupled, noncollective excited states, the smoothing of the barrier distribution could be due to the cumulative coupling to these states. Further theoretical investigations [4,5] confirm this explanation for the observed lack of structure in $D_{\rm qe}$ for the ^{20}Ne + ^{92}Zr system. However, as a doubly magic nucleus, ^{208}Pb has a much lower density of noncollective states; therefore, the calculations including them can only slightly smooth the barrier distribution [4]. This suggests that another mechanism is responsible for the barrier smoothing in the ^{20}Ne + ^{208}Pb system.

An obvious candidate for the barrier smoothing effect in this case is the influence of transfer reactions. Therefore, because of relatively weak dissipation due to the noncollective excitations, ^{20}Ne + ^{208}Pb is a convenient system for testing the influence of dissipation via transfer reactions. In a separate experiment, the transfer reaction cross sections at a backward angle and the incident energy corresponding to the calculated (but not observed) structure in $D_{\rm qe}$ for the ^{20}Ne + ^{208}Pb system were measured [30]. The detection angle ($\theta_{\rm lab} = 142.5$ deg) was chosen to lie in the angular range of the flat peak of the transfer angular distributions. In terms of the differential cross section at this angle and beam energy, the essential reactions turned out to be the single-neutron pickup, ^{208}Pb(^{20}Ne, ^{21}Ne) ^{207}Pb, and the single-proton stripping, ^{208}Pb(^{20}Ne, ^{19}F) ^{209}Bi. However, the two-neutron pickup and two-proton stripping transfers were of comparable importance to the single-proton stripping. The production of ejectiles with masses from 14 to 16 was also significant. The relatively large cross sections for transfer reactions suggest that it is at least plausible that they are responsible for the observed barrier smoothing in the ^{20}Ne + ^{208}Pb system. To test this hypothesis, we included the main transfer channels within the microscopic and phenomenological approaches mentioned above.

The paper is organized as follows: Section II describes the coupled reaction channels (CRC) calculations. Section III reports the results of the calculations performed within the phenomenological approach applying the coupled channels (CC) method using an upgraded CCQEL code [31]. We give the conclusions and summary in Sec. IV.

II. MICROSCOPIC APPROACH

The CRC calculations were carried out using the code FRESCO. The couplings to the 1.63 MeV 2^+ and 4.25 MeV 4^+ states of ^{20}Ne and the 2.62 MeV 3^- state of ^{208}Pb were included. The collective model was assumed, and the ^{20}Ne states were considered to form part of the ground state rotational band, while the ^{208}Pb 3^- was modeled as a single octupole phonon state. The influence of other states and mutual excitations can be considered negligible [29]. Single-neutron pickup and single-proton stripping were included since these are the strongest transfer channels. On the other hand, despite the significant transfer strength of the two-neutron pickup and stripping channels, their couplings were not included because of the lack of necessary experimental spectroscopic amplitudes for the sequential transitions involving excited states in the intermediate and final channels. For similar reasons, we neglected the α-particle stripping and breakup and two-step transfer paths for the single–neutron pickup and single-proton stripping, i.e., excitation of the 2^+ state of ^{20}Ne followed by the transfer step.

The optical potentials in all channels consisted of double-folded real and "interior" imaginary parts, the latter to simulate the incoming-wave boundary condition [29]. The imaginary parts were of Woods-Saxon form, with depth $W = 50$ MeV, radius $R_W = 1.1 \times (A_p^{1/3} + A_t^{1/3})$ fm, and diffuseness $a_W = 0.4$ fm. The double-folded real parts were calculated with the code DFPOT [32] using the energy-independent form of the $M3Y$ effective interaction [33] and nuclear matter densities taken from Ref. [34] for ^{208}Pb and calculated according to the liquid-drop model of Myers [35] for ^{207}Pb and ^{209}Bi. The ^{20}Ne and ^{21}Ne matter densities were calculated according to the prescription of Bhagwat *et al.* [36], assuming a ^{20}Ne $+n$ cluster structure for ^{21}Ne, while the ^{19}F matter density was derived from the charge density of Hallowell *et al.* [37].

For the Coulomb excitation of ^{20}Ne, we took the necessary $B(E2)$ and $B(E4)$ values from Ref. [38], while the ^{208}Pb $B(E3)$ value is from Ref. [39]. We adopted a different approach to the usual deformed potential model for nuclear excitation. There is considerable scatter in the nuclear deformation lengths for ^{20}Ne extracted from different experiments using this model, e.g., Blanpied *et al.* [40]. It has been found that not only is the deformed potential model increasingly inadequate as the multipolarity of the transition increases (see Ref. [41] and references therein), but also the multipole moments of the inelastic transitions are usually much more consistently defined by different data sources, e.g., the review by Mackintosh [42]. We, therefore, employed the double-folding model to calculate the nuclear transition form factors. No imaginary couplings were included due to the interior nature of the entrance channel's imaginary potential, thus avoiding the problem of defining these form factors (the M3Y effective interaction being purely real).

Spectroscopic factors for the ^{20}Ne $\rightarrow$ ^{21}Ne transitions we took from Fortier *et al.* [43]. Pickup to the $5/2^+$ and $1/2^+$ states of ^{21}Ne, at 0.35 and 2.80 MeV, respectively, was included, as these are the strongest individual single-neutron states. Spectroscopic factors for the ^{20}Ne $\rightarrow$ ^{19}F transitions were taken from Table 2 of Kaschl *et al.* [44]. Stripping to

TABLE I. States in ^{207}Pb and ^{209}Bi coupled to in the CRC calculations. The cross sections for populating the individual states (summed over the states in ^{21}Ne and ^{19}F) at $E_{\rm beam} = 103$ MeV for calculations with "interior" and "tuned" exit channel imaginary potentials are denoted by σ and σ', respectively (see text for details).

^{207}Pb	σ (mb)	σ' (mb)	^{209}Bi	σ (mb)	σ' (mb)
0.00 MeV $1/2^-$	31.1	25.0	0.90MeV $7/2^-$	12.0	12.4
0.57MeV $5/2^-$	33.1	26.0	2.83MeV $5/2^-$	1.75	1.85
0.90MeV $3/2^-$	19.7	16.6	3.12MeV $3/2^-$	2.40	2.55
1.63MeV $13/2^+$	2.38	1.91	3.63MeV $1/2^-$	0.40	0.43
2.34MeV $7/2^-$	3.38	2.96			

the $1/2^+$, $1/2^-$, and $5/2^+$ states (at 0.0, 0.112, and 0.198 MeV) of ^{19}F was included. Transitions to the states in ^{207}Pb and ^{209}Bi listed in Table I were included, with spectroscopic factors taken from Refs. [45] and [46], respectively.

Figure 1(a) compares the calculated quasielastic scattering excitation functions with the measured ones. Experimentally, the quasielastic scattering is defined as the sum of all observed direct reaction channels (i.e., elastic and inelastic scattering, transfer, and breakup, where present) [29]. On the other hand, the calculated quasielastic scattering is the sum of all the direct channels included in the calculation. Therefore, the calculated quasielastic scattering excitation function should slightly underpredict the measured one. The corresponding quasielastic barrier distributions $D_{\rm qe}$ are presented in Fig. 1(b). Both excitation functions and barrier distributions are shown as a function of the effective energy $E_{\rm eff}$, defined as in [47] to remove the dependence on scattering angle due to centrifugal effects. However, due to residual differences in $E_{\rm eff}$ for different angles, the correction for the angle-dependent centrifugal energy is not as suitable in this case as it was for other systems. Therefore, the calculations are compared with the experimental results for $\theta_{\rm lab} = 155$ deg only.

The quasielastic excitation function calculated with inelastic couplings [see Fig. 1(a)], except for the high energy tail, is in decent agreement with the measured one. The theoretical calculations were shifted of 2.5 MeV to better compare the shapes with the experimental data. Including the (^{20}Ne, ^{21}Ne) and (^{20}Ne, ^{19}F) transfer channels improves somewhat the qualitative agreement of the calculated excitation function with the measured one. The main qualitative difference between the calculated and measured excitation functions is the "shoulder" at $E_{\rm eff} \approx 95$ MeV, which is absent in the experimental data. This disagreement is much better seen in the barrier distributions plotted in Fig. 1(b), which is associated with the peak in the calculated distribution centered around $E_{\rm eff} = 93$ MeV, produced by the strong coupling to the ^{20}Ne 2_1^+ state. Figure 1(a) shows that the slight smoothing out of the shoulder in the excitation function by the transfer couplings is due to the shifting and broadening of the main peak in the barrier distribution (centered at $E_{\rm eff} \approx 95$ MeV in the calculation) rather than any suppression of the subsidiary

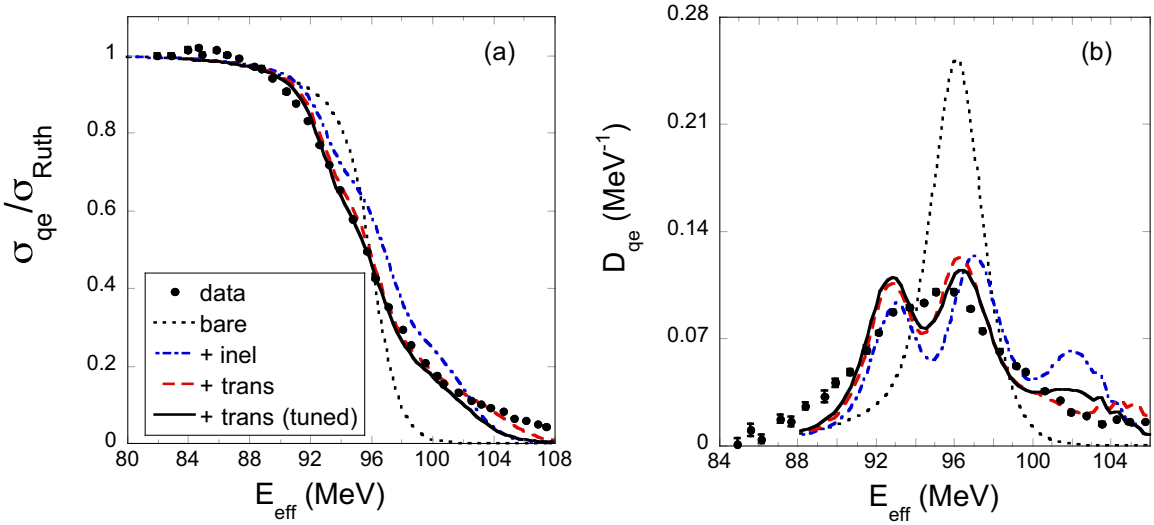

FIG. 1. Theoretical quasielastic excitation functions (a) and quasielastic barrier distributions ($D_{\rm qe}$) (b) compared with the experimental data. The black dotted and blue dot-dashed curves denote the bare (no-coupling) calculation and the calculation with inelastic couplings to the ^{20}Ne 2_1^+ and 4_1^+ and ^{208}Pb 3_1^- states only, respectively. The red dashed and black solid curves denote the complete CRC calculations with "interior" imaginary potentials in all channels and "tuned" imaginary potentials in the ^{21}Ne + ^{207}Pb and ^{19}F + ^{209}Bi exit channels, respectively (see text for details). For the calculated barrier distributions, the experimental resolution of 0.7 MeV (FWHM) was taken into account. The theoretical curves were shifted to higher energy by 2.5 MeV.

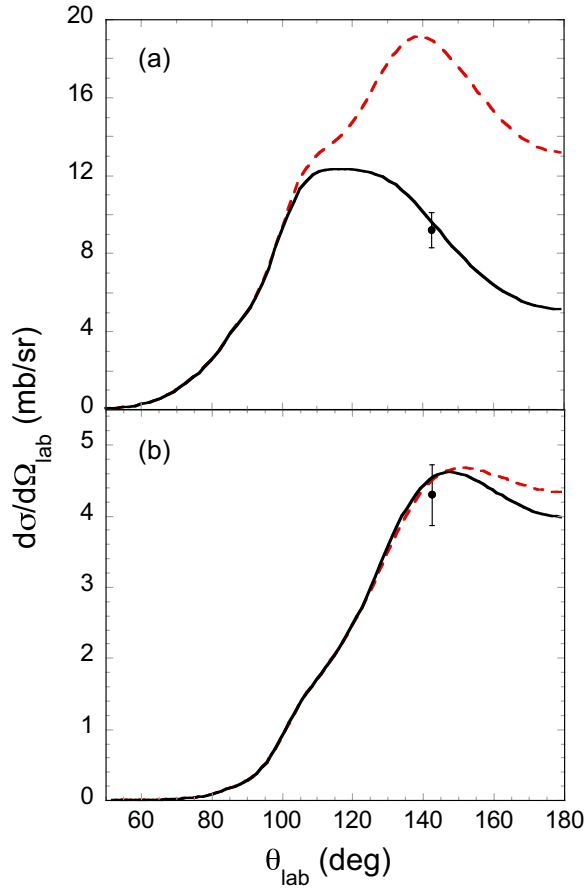

FIG. 2. Transfer angular distributions for the ^{208}Pb(^{20}Ne, ^{21}Ne)^{207}Pb (a) and ^{208}Pb(^{20}Ne, ^{19}F)^{209}Bi (b) reactions summed over all final states. The dashed curve denotes the result of the calculation with interior imaginary potentials in all channels, and the solid curve is the calculation with "tuned" imaginary potentials in the ^{21}Ne + ^{207}Pb and ^{19}F + ^{209}Bi channels (see text for details).

^{20}Ne 2_1^+ peak, which is essentially unaffected by the transfer couplings.

Thus far, we took the transfer coupling strengths—spectroscopic factors and the like—from the literature. However, these values were derived from different reactions. Furthermore, employing "interior" imaginary potentials implies that the surface absorption in all channels must come from explicit couplings. Therefore, the strengths may not accurately reflect the actual transfer cross sections. This could have considerable bearing on the quasielastic barrier distributions, not only through the influence of the coupling effect on the elastic scattering but also on the magnitude of the transfer contribution to the quasielastic scattering. In Fig. 2, the calculated angular distributions are compared with the measured differential cross sections for the ^{208}Pb(^{20}Ne, ^{21}Ne)^{207}Pb and ^{208}Pb(^{20}Ne, ^{19}F)^{209}Bi transfer reactions summed over all states in the residual nuclei at an incident energy of 103 MeV and an angle of $\theta_{lab} = 142.5$ deg. The calculated angular distributions were converted to the laboratory frame and then summed over all states to accurately compare with the measured quantities. Table I reports the integrated cross sections for populating individual states in ^{207}Pb and ^{209}Bi (summed over the relevant states in ^{21}Ne and ^{19}F, respectively) in the column labeled σ'.

It is apparent from Fig. 2 that while the ^{208}Pb(^{20}Ne, ^{19}F)^{209}Bi cross section is well described with the use of "interior" imaginary potentials in all channels, the ^{208}Pb(^{20}Ne, ^{21}Ne)^{207}Pb reaction is significantly overpredicted. The most likely cause of this overprediction is using the interior imaginary potentials in the exit channels. The number of open channels in the ^{21}Ne + ^{207}Pb exit partition, combined with possible interchannel inelastic couplings, is such that it is impossible to include them all in a practical coupled reaction channels calculation. Therefore, adjustments to the optical potential must approximate the effect of these "missing" channels and couplings. The imaginary potential parameters of the exit channel optical potentials were adjusted to obtain a good description of the available transfer data while retaining the interior imaginary potential in the entrance channel. Then, we used the exit channel potential parameters to recalculate the quasielastic excitation function. The results of the calculations with adjusted exit channel optical potentials are compared to the experimental transfer cross section at $E_{beam} = 103$ MeV in Fig. 2, where the solid lines denote them. The integrated cross sections for populating individual states are reported in the column labeled σ' of Table I. The adjusted imaginary potential parameters were $W = 50$ MeV, $r_W = 1.26$ fm, $a_W = 0.4$ fm for the ^{21}Ne + ^{207}Pb partition and $W = 50$ MeV, $r_W = 1.15$ fm, $a_W = 0.4$ fm in the ^{19}F + ^{209}Bi partition. The quasielastic excitation function and barrier distribution obtained from the calculation with "tuned" exit channel optical potentials are compared with the data in Figs. 1(a) and 1(b), respectively, where the solid curves denote them. Figure 1(a) shows that while the qualitative agreement of the tuned calculation with the measured excitation function is somewhat improved, the quantitative agreement is similar to the previous calculation with interior imaginary potentials in all channels. The improved shape of the excitation function is reflected in the calculated barrier distribution of Fig. 1(b), which is in better agreement with the measured one. However, it is readily apparent that despite the included transfer couplings smoothing out to some extent the "two-peak" structure produced by the ^{20}Ne inelastic couplings, a satisfactory description of the measured barrier distribution is not achieved, and this conclusion is unaffected by the quality of the description of the absolute magnitude of the transfer cross sections.

III. PHENOMENOLOGICAL APPROACH

A phenomenological approach was applied by improving the treatment of the transfer couplings in the CC calculations. To this end, we used the CCQEL code, a modified version of the CCFULL code [31], suitable for the fusion and the quasielastic scattering excitation functions to be calculated simultaneously. The improvements aim to take into account experimental information about the dissipation due to the transfer channels. The main difference between the two codes concerns the boundary condition: in CCFULL the incoming

wave boundary condition is applied, while in CCQEL the imaginary potential W is used. Usually, $W(r)$ is, however, hidden behind the barrier, so its details do not influence the fusion cross-section significantly. Before the upgrade, both codes included the two-neutron transfer channels, treated as pair-transfer coupling between the ground states. Under this condition, one usually assumes that transfer coupling is expressed as

$$F_{\rm tr} \times \frac{dV_n}{dr}, \tag{1}$$

where V_n is the nuclear potential [48,49]. The coefficient $F_{\rm tr}$ is the coupling strength, and according to this model, it is independent of

(1) the type of the transferred light particle(s);
(2) the Q value of the reaction (usually g.s. to g.s. transfer (Q_{gg}) is assumed, independently of the projectile energy).

Moreover, since it is frequently assumed that the two-neutron transfer with positive Q_{gg} dominates, one usually considers only this kind of transfer. While the nuclear potential V is frequently calculated using the popular Akyüz-Winther parametrization [50], the transfer coupling strength $F_{\rm tr}$ is usually fitted in the range 0.0–0.5 fm [24,51,52] to obtain agreement of the transfer excitation function with experiment, or is assumed, e.g., at the value of 0.3 fm [25,53]. Sometimes, this is sufficient to reproduce the enhancement of the experimental fusion excitation function over the theoretical one. However, this method is very approximate.

Fusion and quasielastic barrier distributions are frequently, as expected, *grosso modo* similar. However, they could be different in detail due to the different time scales of fusion and scattering, and in particular, of dissipation processes in the reactions [54,55]. In this perspective, the backscattering method offers the possibility of determining the Q-value distribution easily, contrary to the fusion, where only the fixed final Q-values are known.

The Q-value distributions for various transfer channels have been measured in the backscattering of the ^{20}Ne + ^{208}Pb system [30]. We present the results for several transfer channels at the two beam energies of 96 and 103 MeV in Fig. 3. Measurements of the Q-value distribution for transfers at near-barrier energies are rare. However, they almost always have a significant part above the Q_{gg} value, corresponding to negative excitation energy E^* [56,57]. This nonphysical effect was also observed in our measurements. It results from the experimental energy resolution, which for our ^{20}Ne + ^{208}Pb Q distribution measurements was 2.4 MeV (FWHM). Thus, to exploit the information contained in the Q distributions, we performed the deconvolution of experimental Q-value distributions, considering the cutoff at Q_{gg}, i.e., at $E^* = 0$. Some information on the deconvolution method, with examples of the effect of deconvolution on the Q distributions, is given in Appendix A.

The modified CCQEL code, used in this work, allows one to

(1) specify the mass and atomic numbers of the transfer particles;

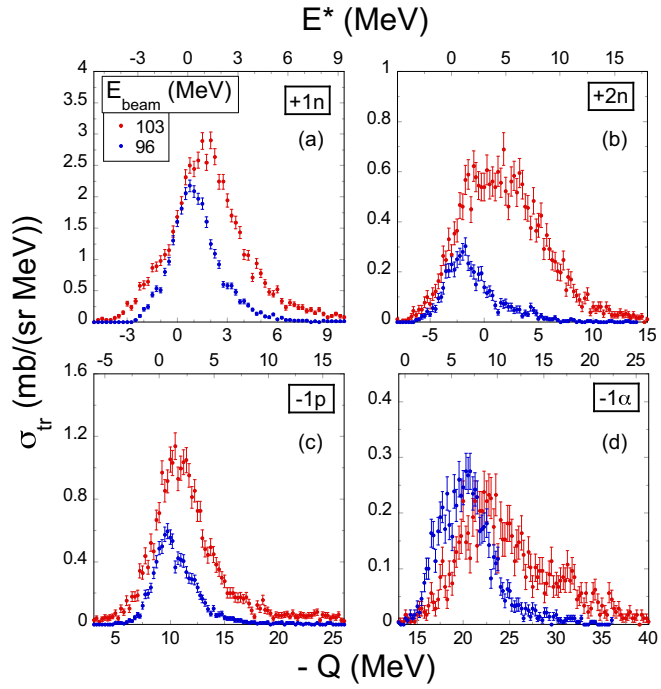

FIG. 3. Q-value distributions for the strongest transfer channels at 96 and 103 MeV beam energies.

(2) include simultaneously various transfer channels;
(3) perform simultaneous calculations with various Q and $F_{\rm tr}$ values based on experimental Q-value distributions.

Comparing the experimental transfer cross section corresponding to some Q values to the calculated ones gives us the $F_{\rm tr}(Q)$ values. The idea is illustrated in Fig. 4. We emphasize that this graph illustrates the idea only in the case of some dominating transfer channel. In practice, we simultaneously

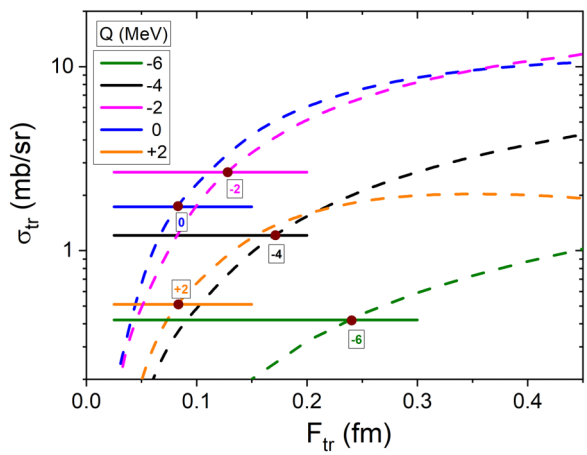

FIG. 4. Principle of the $F_{\rm tr}$ determination for the $+1n$ transfer reaction at the beam energy of 103 MeV. The straight lines give experimental transfer cross sections at a given Q value; the dashed ones are the results of the CCQEL calculations.

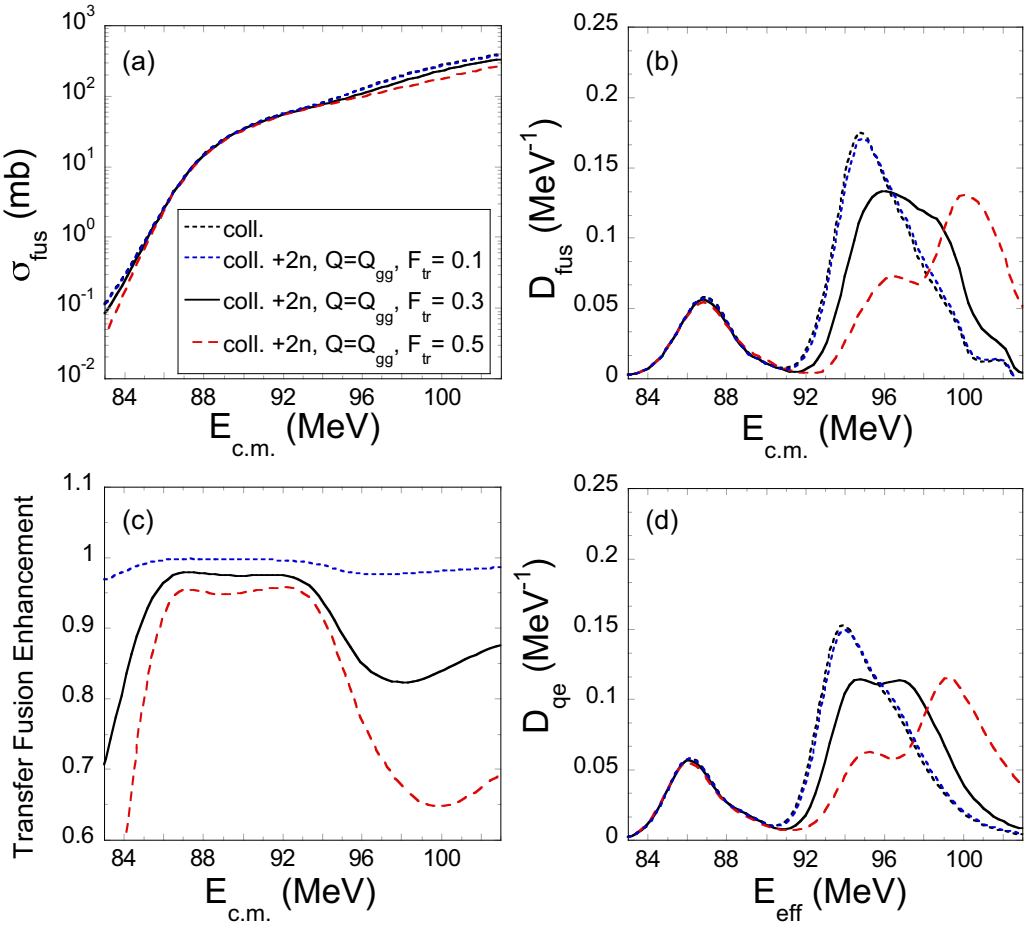

FIG. 5. CC calculations for the ^{20}Ne + ^{208}Pb system performed with standard CCQEL code, including only the collective excitations (dashed black line) and the two-neutron pickup employing fixed F_{tr} values of 0.1 fm (dotted blue line), 0.3 fm (solid black line), and 0.5 fm (dashed red line).

determined the $F_{tr}(Q)$ for a few transfer reactions to reproduce experimental Q-value distributions (see Appendix B).

The ion-ion potential used in the calculation was of the Woods-Saxon shape. In detail, the Akyüz-Winther potential parameters were $V_0 = 69.3$ MeV, $r_0 = 1.18$ fm, and $a = 0.66$ fm for the real part, and $W_0 = 30$ MeV, $r_{0W} = 0.9$, fm and $a_W = 0.5$ fm for the imaginary part. The "interior" imaginary potential simulates the incoming-wave boundary condition. For collective excitations, we have included couplings to the first 3^- state at 2.614 MeV and the first 2^+ state at 4.07 MeV in ^{208}Pb within the two- and one-phonon vibrational coupling schemes, respectively. The deformation parameters of $\beta_3 = 0.11$ and $\beta_2 = 0.055$ [39,58] were used (with the radius parameter for the coupling being 1.2 fm). The calculations included also the couplings between the 0^+, 2^+, 4^+, and 6^+ states in the ^{20}Ne rotational band. The large deformation parameters for ^{20}Ne, $\beta_2 = 0.46$ and $\beta_4 = 0.27$ [40], were employed.

To check the influence of the transfer made in the usual way, the coupled-channels calculations, employing the standard CCQEL code, were performed assuming the ground state to ground state $2n$ pickup with the Q value of 3.02 MeV. We show the results for the three F_{tr} parameters in the 0–0.5 fm range. Figure 5 shows the impact of the assigned F_{tr} values on the fusion excitation function and fusion and quasielastic barrier distributions of the ^{20}Ne + ^{208}Pb systems. The fusion cross sections are smaller at energies above and below the barrier for the strongest coupling ($F_{tr} = 0.5$ fm). This effect is more clearly visible by plotting the transfer fusion enhancement (TFE) [Fig. 5(c)], defined as the ratio of the theoretical estimation of fusion cross sections calculated with and without the transfer channels coupled to the collective excitations. The coupling to the transfer channel slightly affects the barrier distributions' structure. Only in the case of very strong coupling is the peak shape at about 95 MeV more significantly modified. Then, in addition to the collective excitations of projectile and target nuclei, we took into account the dominating transfer channels, where the corresponding F_{tr} values were obtained via the iteration procedure aiming to minimize the difference between the calculated and deconvoluted experimental Q value distributions (the procedure is shortly described in Appendix B).

Figure 6 shows the influence of the two-neutron pickup on the fusion and quasielastic barrier distributions using the standard and upgraded CCQEL codes. For the standard calculations a fixed F_{tr} of 0.3 fm and $Q = Q_{gg}$ were assumed, while for

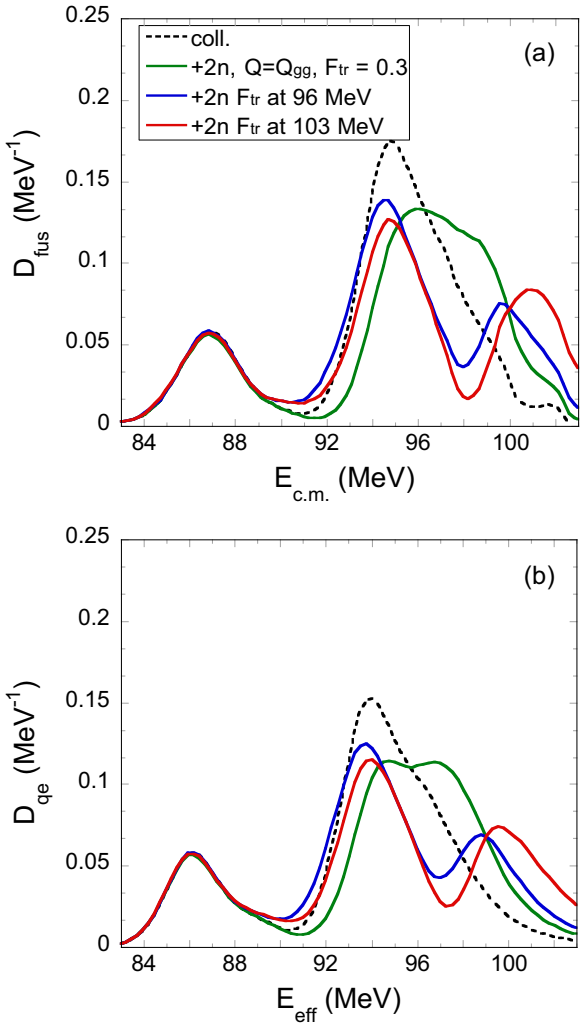

FIG. 6. Comparison of the fusion and quasielastic barrier distributions for the $^{20}\mathrm{Ne}+{}^{208}\mathrm{Pb}$ system obtained with the calculations including the collective excitations (dashed black line) and the two-neutrons pickup. The influence of the transfer channel coupling was calculated with the standard CCQEL code (green solid line) and the upgraded one using the F_{tr} parameters reproducing the experimental Q distributions measured for the beam energies of 96 MeV (blue solid line) and 103 MeV (red solid line) (see details in the text).

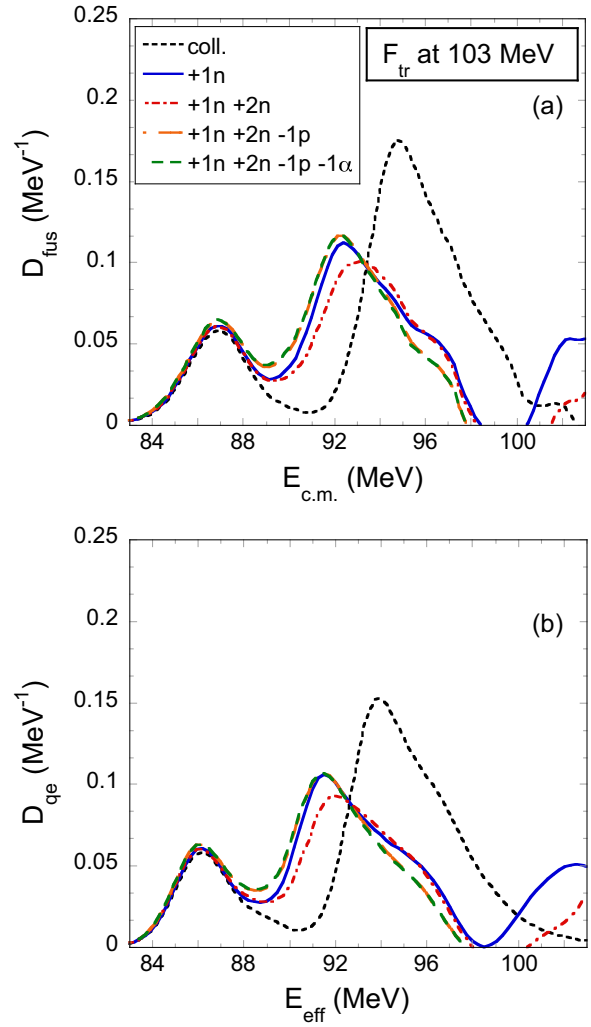

FIG. 7. Comparison of the fusion and quasielastic barrier distributions obtained within the CCQEL code including only the collective excitations (dashed black line) and by gradually including the four strongest transfer reactions starting from the one-neutron pickup: $+1n$ transfer (blue solid line), $+1n$ and $+2n$ transfers (red dash-dotted line), $+1n$, $+2n$, and $-1p$ transfers (orange dashed line), and $+1n$, $+2n$, $-1p$, and -1α transfers (green dashed line). The $F_{\mathrm{tr}}(Q)$ values were obtained from the experimental Q distributions measured at the beam energy of 103 MeV.

the upgraded code the $F_{\mathrm{tr}}(Q)$ values were obtained using the iterative procedure from the experimental Q distributions. In particular, since the transfer cross sections were measured at two beam energies, two sets of $F_{\mathrm{tr}}(Q)$ were obtained. Compared to the calculations, where the coupling to the transfer was neglected, the standard $2n$ treatment of the transfer coupling generates barrier distributions slightly smoothed. At the same time, the upgraded method leads to the splitting of the higher energy peak of both fusion and quasielastic barrier distributions into two peaks. No changes are observed in the shape and position of the lower energy peak.

Generally, it seems that the $2n$ pickup does not significantly smooth out the barrier distributions. This observation suggests that the smoothing is the dissipation effect due to all transfer channels, which strongly influence the barrier distributions. Figure 7 shows such an effect by comparing the fusion and quasielastic barrier distributions obtained by gradually including the four strongest transfer reactions starting from the one-neutron pickup. Because of the two beam energy measurements, the comparison is performed for the F_{tr} obtained separately at 96 and 103 MeV (Figs. 7 and 8, respectively). At beam energies above the barrier, the influence of one-neutron pickup seems to dominate the other transfer channels. The couplings to the $+1n$ transfer lead to the significant smoothing of the two peaks structure of the barrier distributions, while the other transfer channels only slightly influence the structure established by the one-neutron pickup (see Fig. 7). Different situations appear at energies below the barrier, where the one-neutron pickup and one-proton stripping strongly modify the

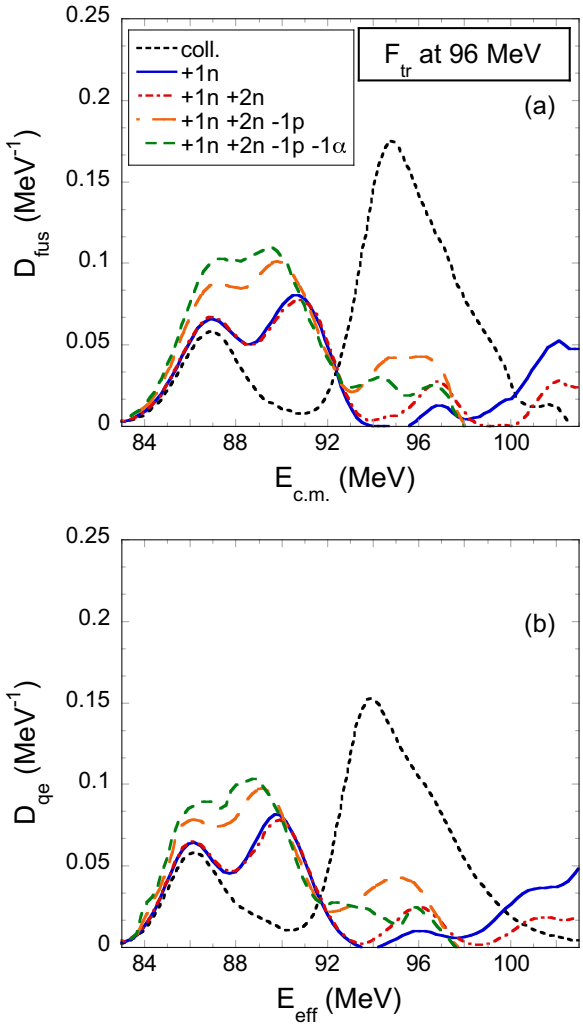

FIG. 8. Comparison of the fusion and quasielastic barrier distributions obtained within the CCQEL code including only the collective excitations (dashed black line) and by gradually including the four strongest transfer reactions starting from the one-neutron pickup: $+1n$ transfer (blue solid line), $+1n$ and $+2n$ transfers (red dash-dotted line), $+1n$, $+2n$, and $-1p$ transfers (orange dashed line), and $+1n$, $+2n$, $-1p$, and -1α transfers (green dashed line). The $F_{\rm tr}(Q)$ values were obtained from the experimental Q distributions measured at the beam energy of 96 MeV.

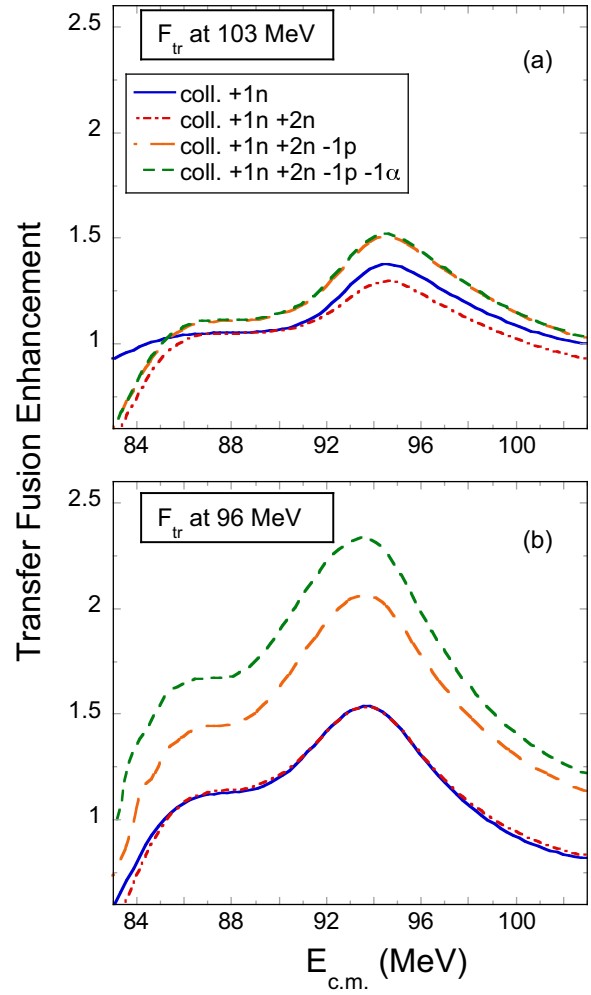

FIG. 9. Comparison of the transfer fusion enhancement obtained within the CCQEL model by including the four strongest transfer reactions starting from the one-neutron pickup: $+1n$ transfer (blue solid line), $+1n$ and $+2n$ transfers (red dash-dotted line), $+1n$, $+2n$, and $-1p$ transfers (orange dashed line), and $+1n$, $+2n$, $-1p$, and -1α transfers (green dashed line). The $F_{\rm tr}(Q)$ values were obtained from the experimental Q distributions measured at the beam energies of 103 (a) and 96 MeV (b).

structure of the barrier distributions by significantly narrowing it, as shown in Fig. 8.

Figure 9 shows the transfer fusion cross-section enhancement obtained by gradually including the four strongest transfer reactions starting from the one-neutron pickup. The comparison highlights the influence of the transfer channel in enhancing the fusion cross-sections mainly at energies near the barrier. As observed by the direct comparison of the barrier distributions, the transfer reactions enhance the fusion cross section for the two beam energies differently. For the beam energy of 96 MeV, the strongest enhancement is due to the one-proton stripping [Fig. 9(b)]; on the other hand, it slightly only influences the fusion cross section at the beam energy of 103 MeV [Fig. 9(a)].

A comparison of calculations with the experimental data is shown in Fig. 10. In general, the coupling to states with a large excitation energy leads to the adiabatic potential renormalization, which consists of an energy-independent shift of the potential [59]. This mainly affects the height of the Coulomb barrier without influencing the trend and shape of the excitation energy and barrier distributions. Thus, we shifted the calculated barrier distributions by 3.7 MeV to overlap with experimental data. The coupling to the four transfer reactions leads to smoother barrier distributions. However, the calculations are still not able to reproduce the experimental data. Furthermore, from the comparison shown in Fig. 10, it is evident how the two sets of coupling strength parameters $F_{\rm tr}(Q)$ obtained for the two beam energies of 96 and 103 MeV generate different fusion and quasielastic barrier distributions and excitation functions. This difference indicates

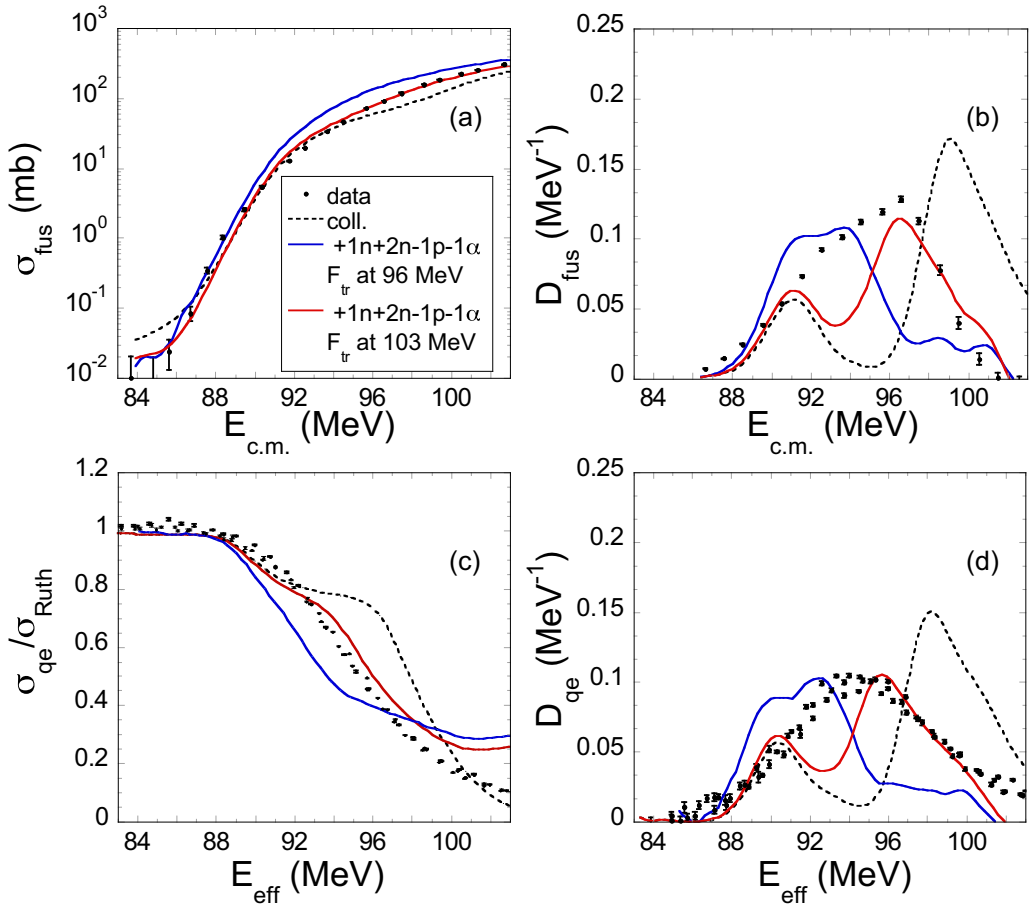

FIG. 10. Comparison of the experimental fusion excitation function (a) and barrier distribution (b) and quasielastic excitation function (c) and barrier distributions (d) for the ^{20}Ne + ^{208}Pb system with the CC calculations performed with only the collective excitations (dashed black line) and the four strongest transfer channels. The $F_{\rm tr}(Q)$ values were obtained from the Q-distribution measurements performed at the beam energies of 96 MeV (blue solid line) and 103 MeV (red solid line). For the calculated barrier distributions, the experimental resolution of 0.7 MeV (FWHM) was taken into account. The theoretical curves were shifted to higher energy by 3.7 MeV.

the coupling strength parameters' strong beam energy dependence, being a direct consequence of the $E_{\rm beam}$ dependence of the Q distributions, presented in Fig. 3. The inclusion of such dependence would probably result in stronger smoothing and broader barrier distributions, observed experimentally. The plateau seen for high $E_{\rm eff}$ in the quasielastic excitation function [Fig. 10(c)], caused mainly by the $-1p$ and -1α transfers high above the barrier, is probably a signal that for high excitation energies the form factor of Eq. (1), even after our generalization, still does not sufficiently well describe the transfer couplings.

IV. SUMMARY AND CONCLUSIONS

A series of microscopic CRC calculations were performed to test the conjecture that couplings to transfer channels could account for the observed smoothing of $D_{\rm qe}$ in the ^{20}Ne + ^{208}Pb system. Couplings to the single-neutron pickup and single-proton stripping channels, experimentally the two strongest transfer reactions, slightly smooth out the structure in the $D_{\rm qe}$ obtained from the microscopic coupled-channels calculations, including the strongest collective states of the projectile and target, but do not provide a satisfactory overall description of the data. This result suggests the importance of the cumulative effect of many individually weak transfer channels, which is responsible for the observed smoothing of $D_{\rm qe}$ in the ^{20}Ne + ^{208}Pb system, rather than the small number of dominating transfer channels. However, including a sufficient number of these weak channels within the framework of a microscopic CRC calculation to unambiguously demonstrate such a smoothing effect remains a practical impossibility for the present, partly due to limitations on the size of a practicable calculation but also to lack of knowledge of the all spectroscopic amplitudes necessary. This latter limitation could, in principle, be overcome by using calculated amplitudes from nuclear structure calculations, although inserting all the necessary transitions into a standard CRC calculation would remain a formidable challenge. Because of this, we upgraded the macroscopic (phenomenological) CCQEL code by improving the coupling method to transfer channels during fusion and backscattering processes.

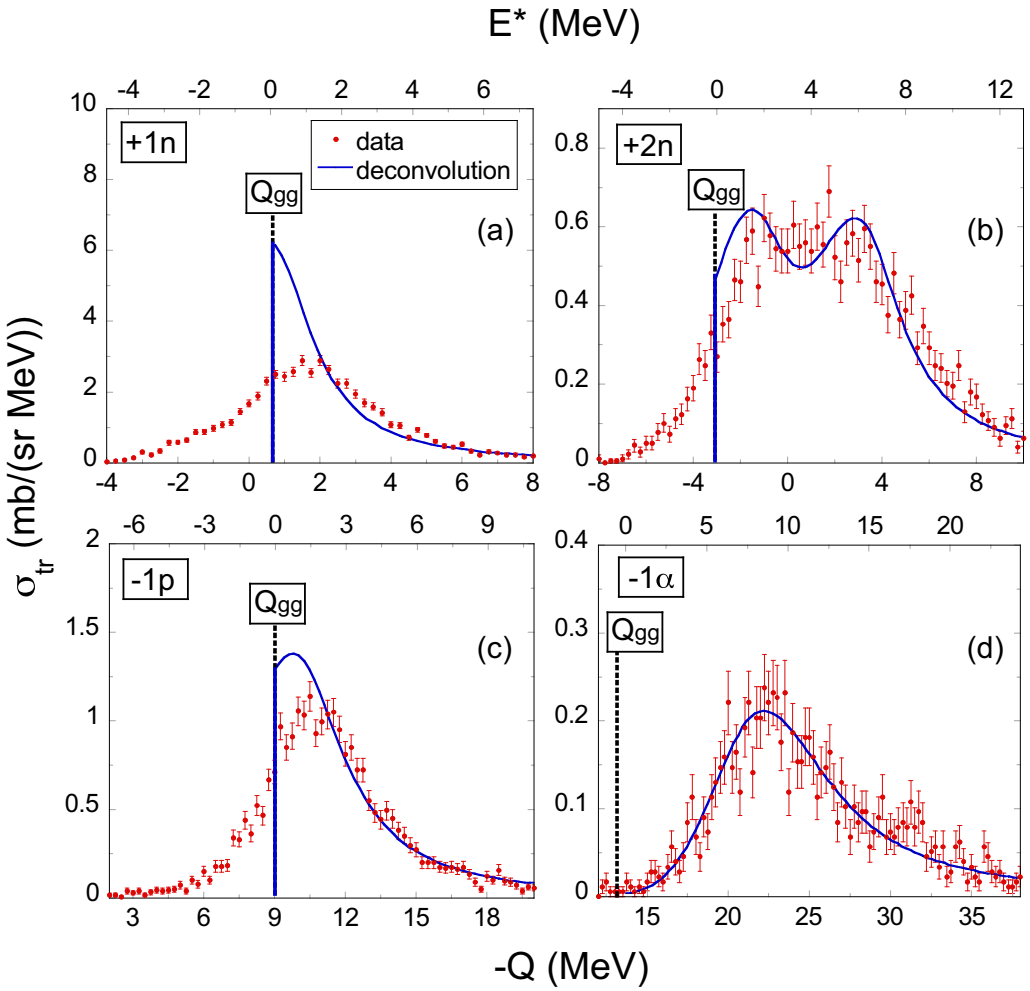

FIG. 11. Examples of deconvolution of the Q-value distributions for the four dominant transfers at the beam energy of 103 MeV.

The upgraded code was employed to investigate the influence of the four main transfer channels on smoothing the measured quasielastic barrier distribution of the $^{20}\mathrm{Ne} + {}^{208}\mathrm{Pb}$ system. The results show significant differences from the ones obtained by applying the standard approximations:

(1) The coupling of transfer channels, at least in the improved CCQEL code's frame, does not strongly enhance the deep sub-barrier fusion cross sections. The enhancement, not larger than by the factor of two (see Fig. 9(b)), was obtained at and slightly below the barrier.

(2) The strongest enhancement is observed not necessarily for $2n$ transfers or transfers with positive Q_{gg} value. For the beam energy of 103 MeV, the smoothing of the barrier distribution is dominated not by $2n$ but rather by $1n$ pickup, even in cases of positive Q_{gg} for $2n$ and negative Q_{gg} for $1n$. On the other hand, for the beam energy of 96 MeV, the $1n$ pickup and $1p$ stripping channels dominate.

(3) In the model's frame, the transfer coupling strength (F_{tr}) depends on the transferred particle and dissipation (Q-value distribution).

(4) The transfer coupling strength F_{tr} depends on the projectile kinetic energy. The two sets of F_{tr} obtained from the Q distributions measured at the two beam energies of 96 and 103 MeV are significantly different. Consequently, the barrier distributions show dissimilar shapes. This effect is a direct consequence of the beam energy dependence of the Q distributions. The introduction of the $F_{\mathrm{tr}}(Q)$ beam energy dependence in the model should lead to the more marked smoothing observed experimentally.

(5) The smoothing is not necessarily dominated by the ground state to ground state transfer. Transfers to higher excited states can also influence it.

(6) Couplings between different transfer channels are essential and, in calculations, should be taken into account.

Since the dissipation due to single-particle excitations and transfers influences the shape of the barrier distributions, in the future, one should develop a code considering dissipation due to the simultaneous single-particle excitations and transfer channels.

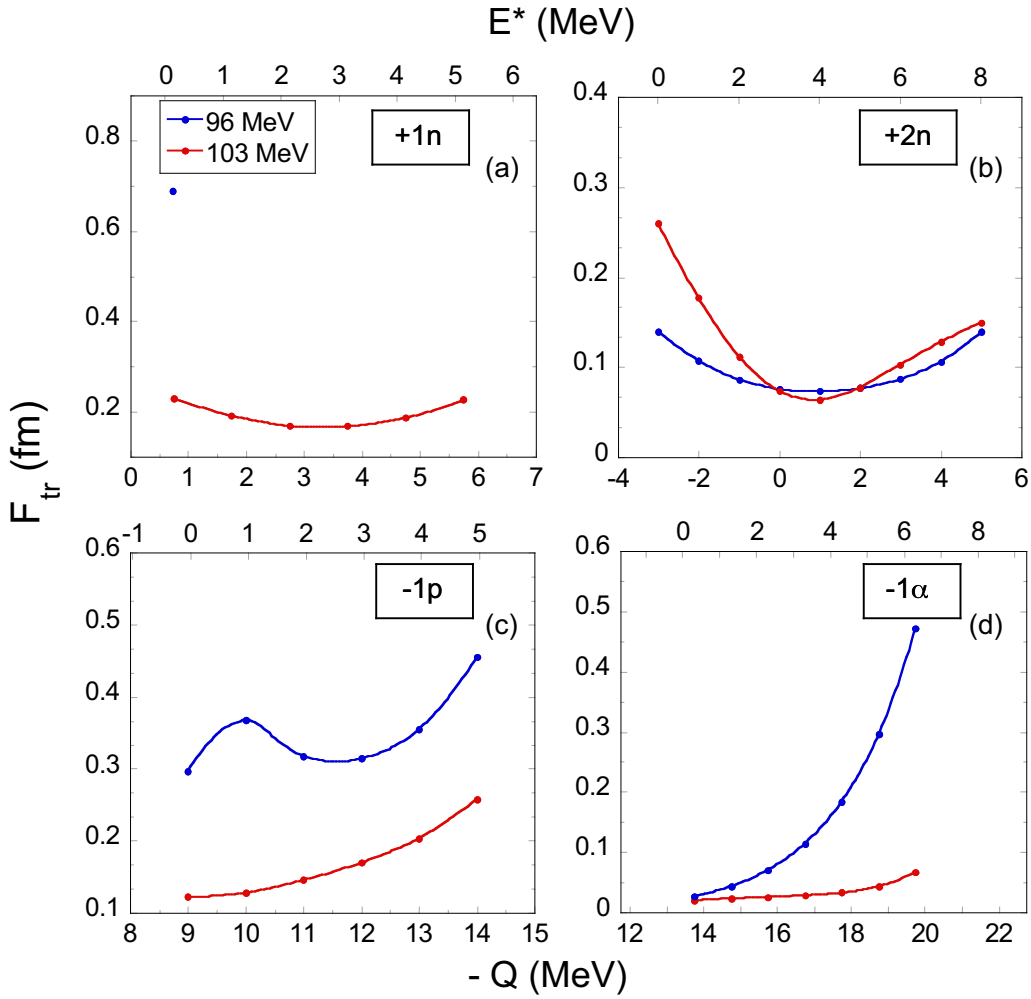

FIG. 12. Dependence of $F_{\rm tr}(-Q, E^*)$ of the four dominant transfer reactions for the two beam energies of 96 MeV (blue solid line) and 103 MeV (red solid line). The single value of $F_{\rm tr}$ for $+1n$ transfer for 96 MeV indicates that, in this case, we see essentially ground state to ground state transfers.

ACKNOWLEDGMENTS

We are grateful to Prof. Keeley for performing the CRC calculations with the FRESCO code and providing a high-level interpretation of the results. We are thankful to Prof. Hagino for his availability and fruitful discussions. This work was partly funded by the SHENG1 project under Contract No. 2018/30/Q/ST2/00163. The work of P.W.W. is supported by the National Natural Science Foundation of China (Grant No. 12375130), and the Director's Foundation of Department of Nuclear Physics, China Institute of Atomic Energy (12SZJJ-202305).

G.C. analyzed the experimental data concerning the transfer cross-section measurement of the ^{20}Ne + ^{208}Pb system. G.C., E.P., and A.T. performed the CC calculations employing the upgraded CCQEL code, interpreted the results, and wrote the paper. P.W.W. developed the upgraded CCQEL code. V.P. and T.A. experimented with the Turchin method of deconvolution in the period December 2020 – September 2021. E.P. implemented the deconvolution procedure.

APPENDIX A: DECONVOLUTION

Deconvolution is the mathematical method aiming to recover the actual physical distribution from experimental results, which are affected by unavoidable experimental resolution, being represented by a distortion function. In the present case, we adopted the Gaussian function, symmetrizing (with respect to the maximum) the negative part of the excitation energy (E^*) distribution obtained for the notransfer reaction and having a standard deviation $\sigma = 1.0$ MeV. Unfortunately, due to the experimental uncertainties, a unique and general method of solving the problem does not exist. An infinite number of solutions exist, evidently nonphysical (e.g., containing many high-frequency oscillations), giving, after convolution with a distortion function, excellent agreement with the experiment. Thus, to get reasonable results, some boundaries should be added, e.g., the condition of nonnegativity of solution for any independent variable value. However, this limitation is frequently insufficient for a unique, physically sound solution. In many applications, one can get a satisfactory solution by adding other conditions, e.g.,

assuming that the solution is smooth [60,61]. Unfortunately, this method cannot be used for the deconvolution of Q-value distributions since, for some transfers, they have a sharp cutoff at Q_{gg} for physical reasons.

Because of this, we used the "Fit Convolution" application of the ORIGINPRO code [62], in which one has to assume the function shape of the solution. We assumed that theleft-hand side of the $E^* = Q_{gg} - Q$ distribution is given by a Gaussian, while the right-hand side is the sum of a Gaussian and Lorentzian, sharply cut at $E^* = 0$. An example of the effect of deconvolution on the Q distributions for the four dominant transfers measured at the beam energy of 103 MeV is presented in Fig. 11. For the $2n$ transfer, where two-peak E^* distribution is evident [see Fig. 11(b)], we assume the sum of two such (Gaussian + Lorentzian) peaks. With such an assumption, we cannot describe the sharp E^* peaks due to the transfers to collective levels, but with our Q-value resolution of the order of 2.4 MeV (FWHM), we could not see them.

APPENDIX B: ITERATION

We determined the transfer coupling strength parameters $F_{\rm tr}(Q)$ for each transfer reaction through an iterative method to minimize the difference between the calculated and experimental Q-value distributions. To this end, the experimental Q distributions were sampled, and a 1 MeV binning was adopted for the studied system. The agreement between the sampled experimental and theoretical Q distributions is established through the factor of agreement, R, which is defined as the ratio of the theoretical (calculated with the updated CCQEL code) and the experimental transfer cross sections. For each iteration, new $F_{\rm tr}^{\rm new}$ parameters were evaluated from the previously used $F_{\rm tr}$ as

$$F_{\rm tr}^{\rm new} = \frac{F_{\rm tr}}{1 - \left(\frac{1-R}{s}\right)}, \tag{B1}$$

where s regulates the step of iteration and was usually set to 4. The iterative procedure ended when the agreement factor R for each transfer and Q was approximately 1. The range of the iterated Q distributions was limited by the possibility of converging the agreement factor R to 1. This mainly affected the alpha transfer channel, where the high energy part of the Q distribution could not be reproduced. However, for other transfers, these limits mainly affected the tails of the Q distributions, whose influence is negligible on the excitation functions and barrier distribution calculations. The $F_{\rm tr}(Q)$ values, which lead to the agreement between theoretical and experimental Q distributions and are employed in the calculations, are shown in Fig. 12. Generally, the $F_{\rm tr}$ parameter strongly depends on the transferred particle and beam energy; the latter one results from the strong beam energy dependence of the Q-value distributions. The dependence of $F_{\rm tr}(-Q, E^*)$ observed for the $1n$ and $2n$ pickups [Figs. 12(a) and 12(b), respectively] suggests that the ground-to-ground state transfer dominates at low excitation energies, but the rising level density amplifies transfer coupling strength at higher excitation energies. With $1p$ and 1α stripping [Figs. 12(c) and 12(d), respectively], the $F_{\rm tr}$ increases with the excitation energy. This might indicate that for the charged particle transfers, the g.s. $\rightarrow$ g.s. channel is not strongly coupled because of the influence of the Coulomb barrier on the charged particles.

[1] M. Dasgupta, D. J. Hinde, N. Rowley, and A. M. Stefanini, Annu. Rev. Nucl. Part. Sci. **48**, 401 (1998).

[2] B. B. Back, H. Esbensen, C. L. Jiang, and K. E. Rehm, Rev. Mod. Phys. **86**, 317 (2014).

[3] E. Piasecki, Ł. Świderski, W. Gawlikowicz, J. Jastrzębski, N. Keeley, M. Kisieliński, S. Kliczewski, A. Kordyasz, M. Kowalczyk, S. Khlebnikov, E. Koshchiy, E. Kozulin, T. Krogulski, T. Loktev, M. Mutterer, K. Piasecki, A. Piórkowska, K. Rusek, A. Staudt, M. Sillanpää *et al.*, Phys. Rev. C **80**, 054613 (2009).

[4] E. Piasecki, M. Kowalczyk, S. Yusa, A. Trzcińska, and K. Hagino, Phys. Rev. C **100**, 014616 (2019).

[5] S. Yusa, K. Hagino, and N. Rowley, Phys. Rev. C **82**, 024606 (2010).

[6] S. Yusa, K. Hagino, and N. Rowley, Phys. Rev. C **88**, 054621 (2013).

[7] S. Yusa, K. Hagino, and N. Rowley, Phys. Rev. C **88**, 044620 (2013).

[8] A. Trzcińska, E. Piasecki, G. Cardella, D. Dell'Aquila, E. De Filippo, S. De Luca, B. Gnoffo, M. Kowalczyk, G. Lanzalone, I. Lombardo, C. Maiolino, N. S. Martorana, A. Pagano, E. V. Pagano, S. Pirrone, G. Politi, L. Quattrocchi, F. Rizzo, P. Russotto, A. Trifiro *et al.*, Phys. Rev. C **102**, 034617 (2020).

[9] L. Corradi, G. Pollarolo, and S. Szilner, J. Phys. G: Nucl. Part. Phys. **36**, 113101 (2009).

[10] Z. Kohley, J. F. Liang, D. Shapira, R. L. Varner, C. J. Gross, J. M. Allmond, A. L. Caraley, E. A. Coello, F. Favela, K. Lagergren, and P. E. Mueller, Phys. Rev. Lett. **107**, 202701 (2011).

[11] L. Corradi, S. Szilner, G. Pollarolo, G. Colò, P. Mason, E. Farnea, E. Fioretto, A. Gadea, F. Haas, D. Jelavić Malenica, N. Mărginean, C. Michelagnoli, G. Montagnoli, D. Montanari, F. Scarlassara, N. Soić, A. M. Stefanini, C. A. Ur, and J. J. Valiente-Dobón, Phys. Rev. C **84**, 034603 (2011).

[12] H. M. Jia, C. J. Lin, F. Yang, X. X. Xu, H. Q. Zhang, Z. H. Liu, L. Yang, S. T. Zhang, P. F. Bao, and L. J. Sun, Phys. Rev. C **86**, 044621 (2012).

[13] G. Montagnoli, A. M. Stefanini, H. Esbensen, C. L. Jiang, L. Corradi, S. Courtin, E. Fioretto, A. Goasduff, J. Grebosz, F. Haas, M. Mazzocco, C. Michelagnoli, T. Mijatovic, D. Montanari, C. Parascandolo, K. E. Rehm, F. Scarlassara, S. Szilner, X. D. Tang, and C. A. Ur, Phys. Rev. C **87**, 014611 (2013).

[14] D. Montanari, L. Corradi, S. Szilner, G. Pollarolo, E. Fioretto, G. Montagnoli, F. Scarlassara, A. M. Stefanini, S. Courtin, A. Goasduff, F. Haas, D. Jelavic Malenica, C. Michelagnoli,

T. Mijatovic, N. Soic, C. A. Ur, and M. Varga Pajtler, Phys. Rev. Lett. **113**, 052501 (2014).
[15] H. M. Jia, C. J. Lin, F. Yang, X. X. Xu, H. Q. Zhang, Z. H. Liu, Z. D. Wu, L. Yang, N. R. Ma, P. F. Bao, and L. J. Sun, Phys. Rev. C **89**, 064605 (2014).
[16] H. Esbensen and A. M. Stefanini, Phys. Rev. C **89**, 044616 (2014).
[17] A. Stefanini, G. Montagnoli, H. Esbensen, L. Corradi, S. Courtin, E. Fioretto, A. Goasduff, J. Grebosz, F. Haas, M. Mazzocco, C. Michelagnoli, T. Mijatović, D. Montanari, G. Pasqualato, C. Parascandolo, F. Scarlassara, E. Strano, S. Szilner, and D. Torresi, Phys. Lett. B **728**, 639 (2014).
[18] A. M. Stefanini, G. Montagnoli, L. Corradi, S. Courtin, D. Bourgin, E. Fioretto, A. Goasduff, J. Grebosz, F. Haas, M. Mazzocco, T. Mijatović, D. Montanari, C. Parascandolo, F. Scarlassara, E. Strano, S. Szilner, N. Toniolo, and D. Torresi, EPJ Web Conf. **86**, 00057 (2015).
[19] G. Scamps and K. Hagino, Phys. Rev. C **92**, 054614 (2015).
[20] D. Montanari, L. Corradi, S. Szilner, G. Pollarolo, A. Goasduff, T. Mijatović, D. Bazzacco, B. Birkenbach, A. Bracco, L. Charles, S. Courtin, P. Désesquelles, E. Fioretto, A. Gadea, A. Görgen, A. Gottardo, J. Grebosz, F. Haas, H. Hess, D. Jelavić Malenica *et al.*, Phys. Rev. C **93**, 054623 (2016).
[21] D. C. Rafferty, M. Dasgupta, D. J. Hinde, C. Simenel, E. C. Simpson, E. Williams, I. P. Carter, K. J. Cook, D. H. Luong, S. D. McNeil, K. Ramachandran, K. Vo-Phuoc, and A. Wakhle, Phys. Rev. C **94**, 024607 (2016).
[22] H. Jia, C. Lin, L. Yang, X. Xu, N. Ma, L. Sun, F. Yang, Z. Wu, H. Zhang, Z. Liu, and D. Wang, Phys. Lett. B **755**, 43 (2016).
[23] H. Jia, C. Lin, L. Yang, X. Xu, F. Yang, N. Ma, L. Sun, D. Wang, Z. Liu, and H. Zhang, Nucl. Phys. Rev. **34**, 361 (2017).
[24] N. K. Deb, K. Kalita, H. A. Rashid, S. Nath, J. Gehlot, N. Madhavan, R. Biswas, R. N. Sahoo, P. K. Giri, A. Das, T. Rajbongshi, A. Parihari, N. K. Rai, S. Biswas, Khushboo, A. Mahato, B. J. Roy, A. Vinayak, and A. Rani, Phys. Rev. C **102**, 034603 (2020).
[25] T. Tanaka, K. Morita, K. Morimoto, D. Kaji, H. Haba, R. A. Boll, N. T. Brewer, S. Van Cleve, D. J. Dean, S. Ishizawa, Y. Ito, Y. Komori, K. Nishio, T. Niwase, B. C. Rasco, J. B. Roberto, K. P. Rykaczewski, H. Sakai, D. W. Stracener, and K. Hagino, Phys. Rev. Lett. **124**, 052502 (2020).
[26] K. Cook, D. Rafferty, D. Hinde, E. C. Simpson, M. Dasgupta, L. Corradi, M. Evers, E. Fioretto, D. Jeung, N. Lobanov, D. H. Luong, T. Mijatovic, G. Montagnoli, A. M. Stefanini, and S. Szilner, Nat. Commun. **14**, 7988 (2023).
[27] I. J. Thompson, Comput. Phys. Rep. **7**, 167 (1988).
[28] E. Crema, B. Paes, V. A. B. Zagatto, J. F. P. Huiza, J. Lubian, J. M. B. Shorto, R. F. Simões, D. S. Monteiro, N. Added, M. C. Morais, and P. R. S. Gomes, Phys. Rev. C **100**, 054608 (2019).
[29] E. Piasecki, Ł. Świderski, N. Keeley, M. Kisieliński, M. Kowalczyk, S. Khlebnikov, T. Krogulski, K. Piasecki, G. Tiourin, M. Sillanpää, W. H. Trzaska, and A. Trzcińska, Phys. Rev. C **85**, 054608 (2012).
[30] E. Piasecki, W. Czarnacki, N. Keeley, M. Kisieliński, S. Kliczewski, A. Kordyasz, M. Kowalczyk, S. Khlebnikov, E. Koshchiy, T. Krogulski, T. Loktev, M. Mutterer, A. Piórkowska, K. Rusek, M. Sillanpää, A. Staudt, I. Strojek, S. Smirnov, W. H. Trzaska, and A. Trzcińska, Phys. Rev. C **85**, 054604 (2012).
[31] K. Hagino, N. Rowley, and A. T. Kruppa, Comput. Phys. Commun. **123**, 143 (1999).
[32] J. Cook, Comput. Phys. Commun. **35**, C-775 (1984).
[33] G. Satchler and W. Love, Phys. Rep. **55**, 183 (1979).
[34] G. Satchler, Nucl. Phys. A **579**, 241 (1994).
[35] W. D. Myers, Nucl. Phys. A **145**, 387 (1970).
[36] A. Bhagwat, Y. K. Gambhir, and S. H. Patil, Eur. Phys. J. A **8**, 511 (2000).
[37] P. L. Hallowell, W. Bertozzi, J. Heisenberg, S. Kowalski, X. Maruyama, C. P. Sargent, W. Turchinetz, C. F. Williamson, S. P. Fivozinsky, J. W. Lightbody, and S. Penner, Phys. Rev. C **7**, 1396 (1973).
[38] Y. Horikawa, A. Nakata, and Y. Torizuka, Prog. Theor. Phys. **49**, 2005 (1973).
[39] T. Kibedi and R. H. Spear, At. Data Nucl. Data Tables **80**, 35 (2002).
[40] G. S. Blanpied, B. G. Ritchie, M. L. Barlett, R. W. Fergerson, G. W. Hoffmann, J. A. McGill, and B. H. Wildenthal, Phys. Rev. C **38**, 2180 (1988).
[41] J. Beene, D. Horen, and G. Satchler, Phys. Lett. B **344**, 67 (1995).
[42] R. S. Mackintosh, Rep. Prog. Phys. **40**, 731 (1977).
[43] S. Fortier, S. Gales, S. M. Austin, W. Benenson, G. M. Crawley, C. Djalali, J. S. Winfield, and G. Yoo, Phys. Rev. C **41**, 2689 (1990).
[44] G. Kaschl, G. Wagner, G. Mairle, U. Schmidt-Rohr, and P. Turek, Nucl. Phys. A **155**, 417 (1970).
[45] M. Franey, J. Lilley, and W. Phillips, Nucl. Phys. A **324**, 193 (1979).
[46] R. Groleau, W. A. Lanford, and R. Kouzes, Phys. Rev. C **22**, 440 (1980).
[47] H. Timmers, D. Ackerman, S. Beghini, L. Corradi, J. H. He, G. Montagnoli, F. Scarlassara, A. M. Stefanini, and N. Rowley, Nucl. Phys. A **633**, 421 (1998).
[48] C. Dasso and G. Pollarolo, Phys. Lett. B **155**, 223 (1985).
[49] C. Dasso and A. Vitturi, Phys. Lett. B **179**, 337 (1986).
[50] O. Akyüz and A. Winther, in *Nuclear Structure and Heavy-Ion Collisions, Proceedings of the International School of Physics "Enrico Fermi", Course LXXVII*, Varenna, Italy, 1979, edited by R. A. Broglia, C. H. Dasso, and R. Ricci (North-Holland, Amsterdam, 1981).
[51] A. M. Stefanini, G. Montagnoli, H. Esbensen, P. Čolović, L. Corradi, E. Fioretto, F. Galtarossa, A. Goasduff, J. Grebosz, F. Haas, M. Mazzocco, N. Soić, E. Strano, and S. Szilner, Phys. Rev. C **96**, 014603 (2017).
[52] R. N. Sahoo, M. Kaushik, A. Sood, A. Sharma, S. Thakur, P. Kumar, M. M. Shaikh, R. Biswas, A. Yadav, M. K. Sharma, J. Gehlot, S. Nath, N. Madhavan, R. G. Pillay, E. M. Kozulin, G. N. Knyazheva, K. V. Novikov, and P. P. Singh, Phys. Rev. C **102**, 024615 (2020).
[53] M. M. Shaikh, S. Roy, A. Mukherjee, A. Goswami, B. Dey, S. Pal, S. Roy, A. Shrivastava, S. K. Pandit, and K. Mahata, Phys. Rev. C **102**, 024627 (2020).
[54] N. Rowley, G. R. Satchler, and P. H. Stelson, Phys. Lett. B **254**, 25 (1991).
[55] H. Timmers, J. R. Leigh, M. Dasgupta, D. J. Hinde, R. C. Lemmon, J. C. Mein, C. R. Morton, J. O. Netwon, and N. Rowley, Nucl. Phys. A **584**, 190 (1995).
[56] T. Mijatović, S. Szilner, L. Corradi, D. Montanari, G. Pollarolo, E. Fioretto, A. Gadea, A. Goasduff, D. J. Malenica, N. Mărginean, M. Milin, G. Montagnoli, F. Scarlassara, N. Soić, A. M. Stefanini, C. A. Ur, and J. J. Valiente-Dobón, Phys. Rev. C **94**, 064616 (2016).

[57] J. Diklić, S. Szilner, L. Corradi, T. Mijatović, G. Pollarolo, P. Čolović, G. Colucci, E. Fioretto, F. Galtarossa, A. Goasduff, A. Gottardo, J. Grebosz, A. Illana, G. Jaworski, M. J. Gomez, T. Marchi, D. Mengoni, G. Montagnoli, D. Nurkić, M. Siciliano *et al.*, Phys. Rev. C **107**, 014619 (2023).
[58] S. Raman, At. Data Nucl. Data Tables **78**, 1 (2001).
[59] K. Hagino and N. Takigawa, Prog. Theor. Phys. **128**, 1061 (2012).
[60] V. Turchin, USSR Comput. Math. Math. Phys. **7**, 79 (1967).
[61] V. F. Turchin, V. P. Kozlov, and M. S. Malkevich, Sov. Phys. Usp. **13**, 681 (1971).
[62] https://www.originlab.com/.